Hydrogen retention in ITER's Diagnostic First Wall submitted to cyclic thermomechanical loadings

Shihao Bian, Jonathan Mougenot, Yann Charles, Xavier Bonnin, Tom Wauters, Richard Pitts

Available online at www.sciencedirect.com

ScienceDirect

Structural Integrity Procedia 00 (2019) 000–000

Structural Integrity Procedia

www.elsevier.com/locate/procedia

23 European Conference on Fracture - ECF23

Hydrogen retention in ITER's Diagnostic First Wall submitted to cyclic thermomechanical loadings

Shihao Bian[a]*, Jonathan Mougenot[a], Yann Charles[a], Xavier Bonnin[b], Tom Wauters[b], Richard Pitts[b]

[a]*Université Sorbonne Paris Nord, Laboratoire des Sciences des Procédés et des Matériaux, LSPM, CNRS, UPR 3407, F - 93430, Villetaneuse, France*

[b]*ITER Organization, Route de Vinon-sur-Verdon, CS 90046, 13067, St. Paul Lez Durance Cedex, France*

Abstract

A simplified ITER's Diagnostic First Wall is modelled in Abaqus Finite Element software to evaluate hydrogen retention after cyclic plasma exposure, and especially, the impact of mechanical fields. Using several User Subroutines, a strongly coupled chemo-thermo-mechanical problem is set and solved. Hydrogen field results with or without mechanical fields are compared, during the different loading phases, leading to the conclusion that, for this simplified problem, mechanical fields have no important impact on hydrogen retention.

Keywords: Hydrogen; Diffusion; Trapping; Thermomechanic; Finite Element; Abaqus

* Corresponding author. Tel: +33-1-49-40-36-25
E-mail address: shihao.bian@lspm.cnrs.fr

1. Introduction

ITER (International Thermonuclear Experimental Reactor) is an international nuclear fusion research and engineering project aimed at replicating the fusion processes of the Sun to produce energy on Earth. The largest nuclear fusion reactor in the world, the ITER tokamak, is under construction.

ITER's Diagnostic First Wall (DFW) structure (Loesser et al., 2017) is composed of structural elements intended to support plasma diagnostic devices and protective panels of the vacuum chamber. These are made of 316L steel, and are subjected to cycles of both heat and particle fluxes (including tritium, a radioactive isotope of hydrogen). These particles may diffuse in the structure and get trapped by material defects (vacancies, dislocations, ...), assisted by thermo-mechanical fields.

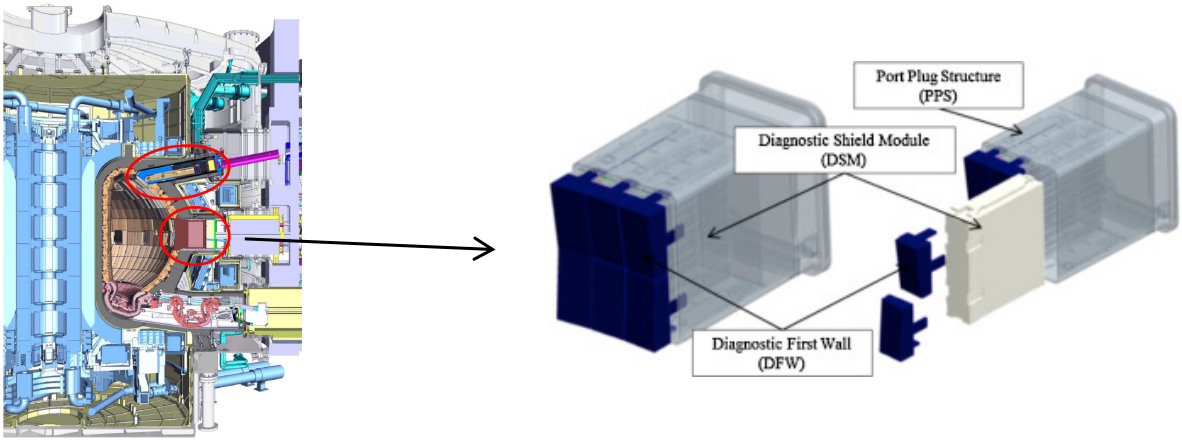

Fig. 1. (a) ITER DFW location (reproduced from (Loesser et al., 2017)); (b) DFW (reproduced from (Giacomin et al., 2015))

Estimating the amount of tritium contained in DFW is mandatory for safety issues and component reliability (e.g., to avoid any Hydrogen Embrittlement-related phenomenon), especially to assess tritium permeation fluxes towards the DFW's cooling pipes, linked to a pollution risk.

If several thermomechanical studies have been performed on this component (Khodak et al., 2017; Smith et al., 2017), to the authors' knowledge, no analysis has yet been provided related to tritium diffusion and trapping in the DFW, with or without accounting for thermal and mechanical fields (Benannoune et al., 2020).

The aim of this study is to model, in Abaqus Finite Element software, tritium transport through a very simplified DFW model, submitted to cycling loadings.

First, the DFW model and the constitutive equations are presented, as well as the modelling strategy. Results are then shown and commented.

Nomenclature

C_L	diffusive hydrogen concentration	A	elastic limit
C_T	trapped hydrogen concentration	B	hardening constant
N_L	interstitial sites density	C	strain rate constant
N_T	trap density	n	hardening exponent
θ_L	interstitial site occupancy	m	thermal softening exponent
θ_T	trap site occupancy	ε_p	equivalent plastic strain
ρ	density	σ_Y	yield stress
C_p	specific heat	T_{room}	room temperature
T	temperature	T_{melt}	melting temperature

λ	thermal conductivity	R_p	particle implantation depth
$\boldsymbol{\varepsilon}_{th}$	thermal strain tensor	φ_{imp}	implantation flux of hydrogen
α	thermal expansion coefficient	D_L	hydrogen diffusion coefficient
$\boldsymbol{I}$	identity tensor	C_{L0}	hydrogen boundary condition

2. Constitutive equations

Several physical phenomena are involved in the problem resolution: hydrogen transport and trapping, mechanical behavior, and heat transfer, all being coupled. In the following, hydrogen is considered instead of tritium.

2.1. Hydrogen transport

It is assumed that the total hydrogen concentration can be split into a diffusive part, C_L, and a trapped one, C_T. If several kinds of traps are involved, $C_T = \sum_i C_{T,i}$, i being the trap kind number. These concentrations are related to trap densities $N_{T,i}$ (or interstitial site density N_L) by the occupancy $\theta_{T,i} \in [0,1]$ (denoted θ_L for diffusive hydrogen):

$$\begin{cases} C_L = N_L \theta_L \\ C_T = \sum_i C_{T,i} = \sum_i N_{T,i} \theta_{T,i} \end{cases} \tag{1}$$

Coupling mechanically-assisted hydrogen flux φ_L (based on Fick's law) (Bockris et al., 1971; Li et al., 1966) and mass conservation yields the diffusion and trapping equation (Sofronis and McMeeking, 1989)

$$\frac{\partial C_L}{\partial t} + \sum_i \frac{\partial C_{T,i}}{\partial t} = \boldsymbol{\nabla}.\left(D_L \boldsymbol{\nabla} C_L + D_L C_L \frac{V_H}{RT} \boldsymbol{\nabla} P_H \right) \tag{2}$$

where R is the ideal gas constant, T the absolute temperature, D_L the hydrogen diffusion coefficient, and V_H the partial molar volume of hydrogen. $P_H = -1/3\ \mathrm{tr}(\boldsymbol{\sigma})$ is the hydrostatic stress, where $\boldsymbol{\sigma}$ is the stress tensor. The temporal evolution of the trapped hydrogen concentration (for each trap) can be computed using the so-called McNabb and Foster equation(McNabb and Foster, 1963), for $C_L \ll N_L$ (or $\theta_L \ll 1$)

$$\frac{\partial C_{T,i}}{\partial t} = \frac{k_i}{N_L} C_L \left(N_{T,i} - C_{T,i} \right) - p_i C_{T,i} \tag{3}$$

where $\mathrm{p_i}$ and k_i are the detrapping and trapping reaction rates.

2.2. Heat transfer

The heat transfer equation is

$$\rho C_p \frac{\partial T}{\partial t} = \boldsymbol{\nabla}.(\lambda \boldsymbol{\nabla} T) \tag{4}$$

where ρ is the density, C_p the specific heat and λ the thermal conductivity. Any temperature variation induces a thermal expansion tensor such as

$$\boldsymbol{\varepsilon}_{th} = \alpha(T - T_{init})\boldsymbol{I} \tag{5}$$

where T_{init} is the initial temperature, and $\boldsymbol{I}$ is the identity tensor.

2.3. Mechanical behavior

Isotropic thermo-elasticity is considered, based on Young modulus E and Poisson ratio ν. Isotropic hardening is assumed, based on a Johnson-Cook law (G. R. Johnson and Cook, 1983)

$$\sigma_Y = \left(A + B\varepsilon_p^n\right)\left(1 - \left(\frac{T - T_{room}}{T_{melt} - T_{room}}\right)^m\right) \tag{6}$$

where σ_Y represents the yield stress and ε_p the equivalent plastic strain. T_{room} and T_{melt} represent respectively the room and melting temperatures (assumed to be equal to 300 and 1356 K respectively). Last, A, B, n and m are material parameters.

2.4. Material parameters

All parameters are extracted from literature. N_L and D_L can be found in (Penzhorn et al., 2012). One trap has been considered, with a trapping energy equal to 0.7 eV (Guillermain, 2016), and a density such that $\log N_T = 25.26 - 2.33e^{-5.5\varepsilon_p}$ site/m^3 (adapted from (Kumnick and H. H. Johnson, 1980) to account for an initial dislocation density equal to 10^{12}-10^{14} m/m^3). Heat transfer parameters have been taken from (Umbrello et al., 2007), with an temperature-independent expansion coefficient (Sayman et al., 2009). Last, thermomechanical parameters have been extracted from (Chandrasekaran et al., 2005; Umbrello et al., 2007).

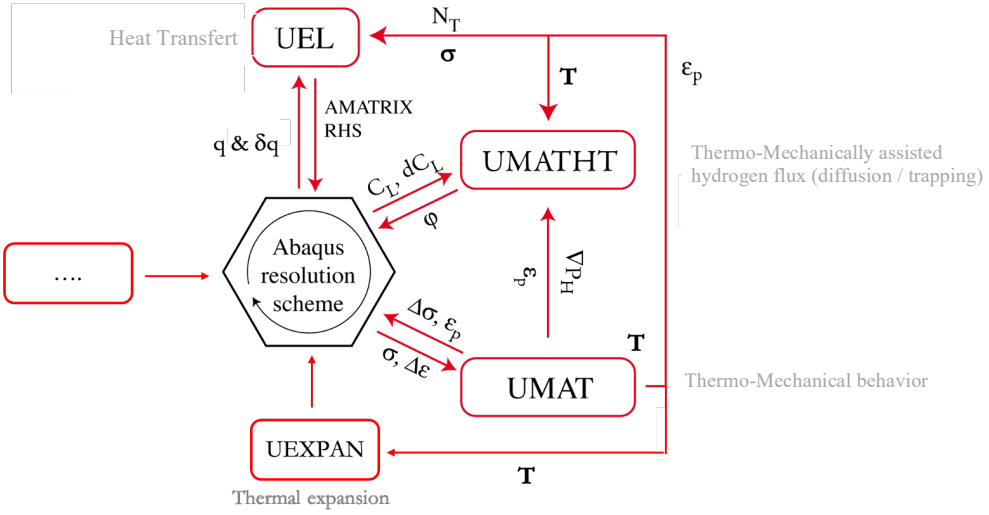

Fig. 2 Implementation scheme of a strongly coupled thermo-chemo-mechanical problem in Abaqus software.

3. Implementation

The chemo-thermo-mechanical system described in the three paragraphs is resolved in a fully coupled way (strong coupling) using the Abaqus Finite Element software (Simulia, 2011), based on the 'coupled temp-displacement' procedure and user subroutines (see (Charles et al., 2017; Vasikaran et al., 2020) for details):

- UMAT subroutine: thermomechanical behavior (section 2.3);
- UMATHT subroutine: hydrogen transport and trapping (section 2.1);
- UEL subroutine: heat transfer (equation (*4*));
- UEXPAN subroutine: thermal expansion (equation (*5*)).

The interactions of the different subroutines are depicted on Fig. 2.

4. Model definition

The geometry of the DFW is presented in Fig. 3(a). For the sake of simplicity, only a part of this geometry will be modelled (indicated by a red rectangle). Each cylindrical conduit represents a tube for the cooling fluid.

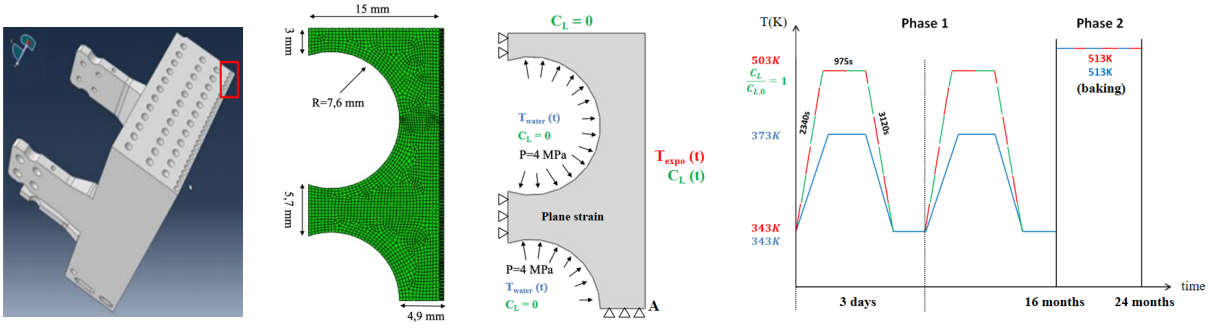

Fig. 3. (a) DFW and the part modelled (in a red rectangle), (b) mesh and dimension, (c) applied boundary conditions. (d) Loading scenario (temperature & hydrogen)

The part of interest is modelled in 2D and meshed with just under 4000 fully integrated linear elements (Fig. 3b). Symmetry boundary conditions are imposed on the lower and left edges (Fig. 3c), and plane strain is assumed. A water flow circulating in the cooling tubes induces a constant pressure on the DFW of 4 MPa. On the plasma-exposed face, heat and hydrogen loading cycles are imposed, while on the upper surface and on the cooling tubes, an instantaneous hydrogen draining is assumed ($C_L = 0$).

The scenario chosen is illustrated in Fig. 3d. It consists of 160 loading cycles of 3 days each (Phase 1), and an annealing cycle of 8 months (Phase 2), at constant temperature and without plasma exposure. Each 3-day cycle corresponds to the temporal concatenation over 3 days of 13 daily plasma pulses of 400 seconds. This cycle is repeated for 16 months (160 cycles). Hydrogen implantation is modelled by a hydrogen concentration C_{L0} on the exposure surface, such as in (Hodille et al., 2018)

$$C_{L0} = \frac{R_p \varphi_{imp}}{D_L} = 1.46 \times 10^{14}\ atom/mm^3 \tag{7}$$

where φ_{imp} represents the hydrogen flux (2×10^{19}atom/m^2/s), R_p represents the average implantation depth (set to 13 nm (Benannoune et al., 2020)).

5. Results

Three calculations were carried out, for the sake of comparison: with no mechanical fields; with only the pressure exerted by the water in the cooling pipes, and considering all thermomechanical fields.

The diffusion fields at the end of Phase 1 are given in Fig. 4 for the three cases. It can be observed that, while the cooling pipes-induced pressure increases the level of C_L, at least near the exposed surface, the depth of C_L's penetration seems not affected by mechanical fields. This impact of the stress field on C_L levels is linked to the hydrostatic pressure

effect on hydrogen flux, which affects the maximal C_L level. To detail that effect, in Fig. 5 are plotted the P_H distributions when only the cooling pipes pressure is considered (Fig. 5a) and with all the mechanical fields, at the higher and lower exposition temperatures (Fig. 5b and Fig. 5c respectively).

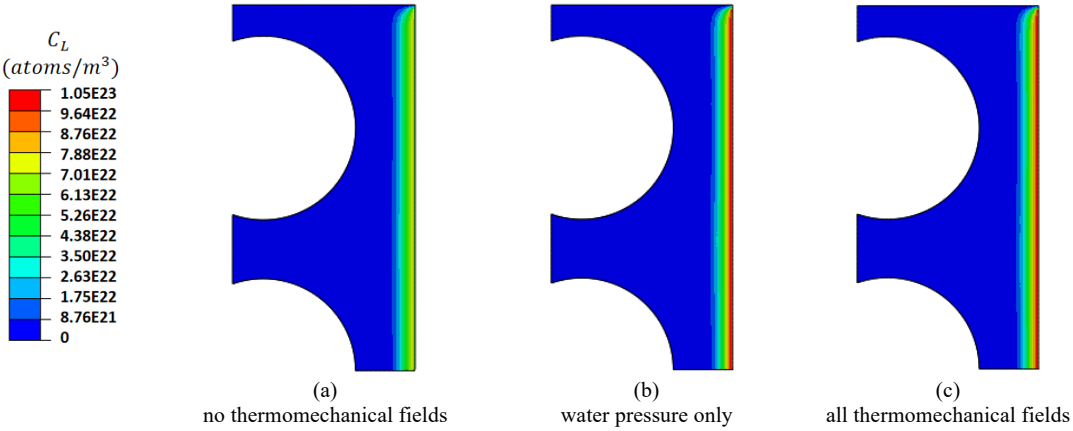

Fig. 4. Distribution of C_L at the end of phase 1 (160 cycles).

When only the water pressure is accounted for, it can be seen that the DFW section is slightly under dilatation (negative pressure), leading to an increase of the C_L maximal value. The extra effect of thermal strains on the C_L field is small, however. During the hot phase of each cycle (higher T_{expo} – see Fig. 3d), two opposite effects are involved: while the important temperature field leads to an increase of the tritium diffusion coefficient, thermal strains (Fig. 6b) induce compression stresses (positive P_H, see Fig. 5b) which tend to slow the tritium diffusion. During the cold phase of each cycle, these two contradictory effects are also present; from the C_L fields, it can be concluded that they neutralize each other, leading to a small overall effect of the thermal strain fields.

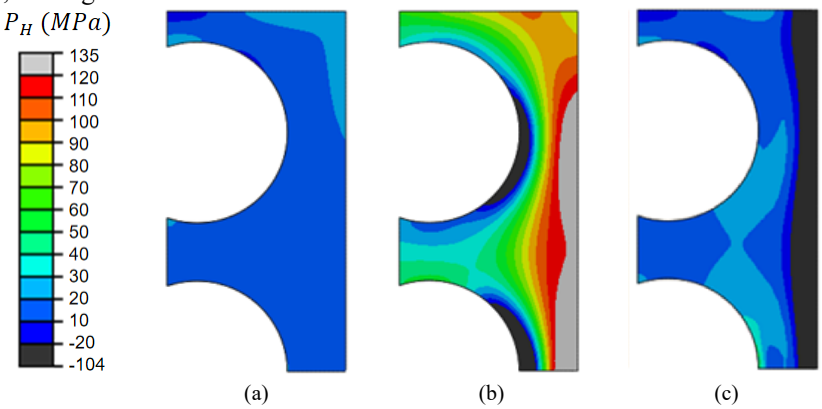

Fig. 5. Distribution of P_H at the end of phase 1's last cycle (160 cycles) considering (a) water pressure only and (b-c) all thermomechanical fields at higher and lower exposition temperature T_{expo} respectively.

The impact of mechanical fields on hydrogen retention can be investigated by introducing its total amount per unit thickness (for a 2D configuration) $Q_{tot} = \int (C_L + C_T) dV$ in the DFW section; Q_{tot} evolution with time is plotted in Fig. 7a for the three cases.

The impact of the cooling pipes pressure is here very clear: at each cycle, Q_{tot} increases continuously, exhibiting cycles corresponding to the plasma loading ones. When the DFW section is exposed to both hydrogen and temperature, Q_{tot} increases. Hydrogen amount decreases as soon as these boundary conditions are modified, during phase 2 (no

more hydrogen concentration and T_{expo}=513 K). This behavior indicates an important hydrogen desorption process, and thus, an important hydrogen mobility. It can last be conjectured that, when the number of cycles increases, so does the maximal Q_{tot} value.

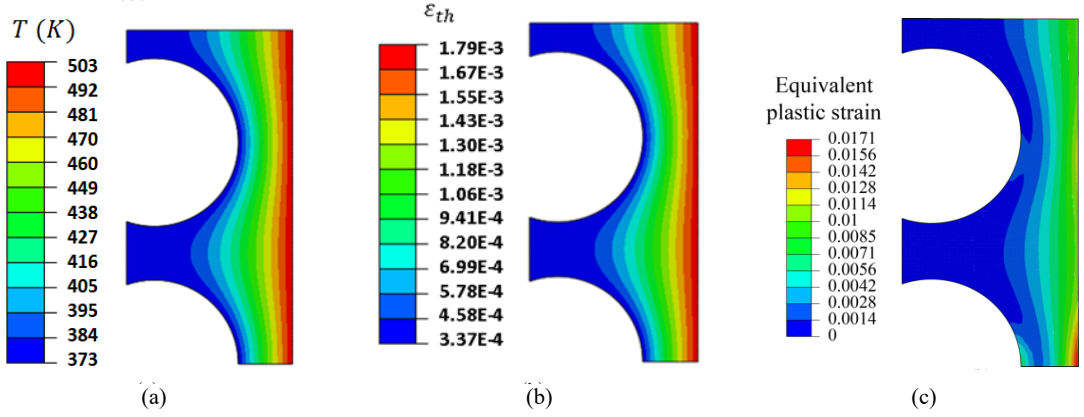

Fig. 6. (a) Temperature and (b) thermal strain fields and (c) equivalent plastic strain at the end of Phase 1's last cycle, at the higher T_{expo} value.

When thermal strain fields are furthermore accounted for, the extra impact on Q_{tot} appears to be small, as previously observed: C_L fields are indeed not that much affected by thermal strains.

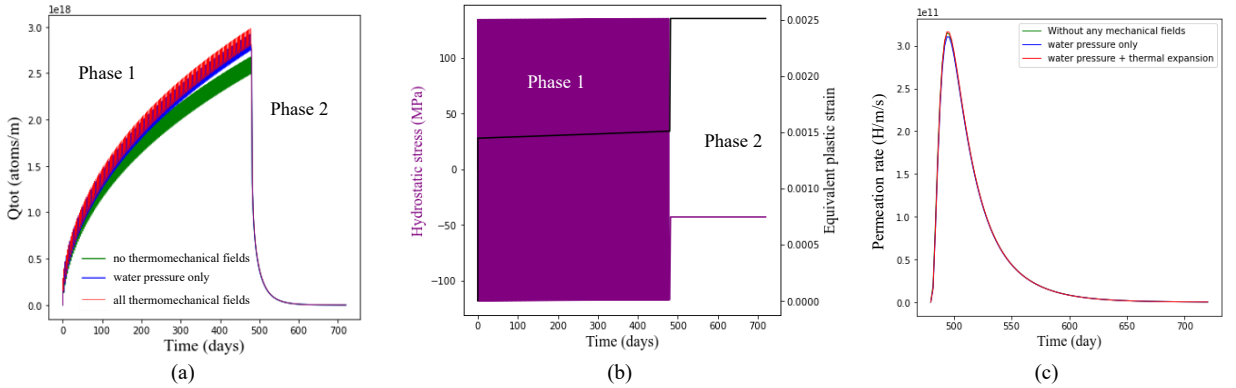

Fig. 7. (a) temporal evolution of the amount of hydrogen $Q_{tot} = \int (C_L + C_T) dV$ per unit thickness for the three configurations, (b) temporal evolution of equivalent plastic strain (black) & hydrostatic stress (purple) at point A (see Fig. 3c) when all thermomechanical fields are resolved. (c) Evolution of the tritium permeation rate during Phase 2 through the cooling pipes.

Thermal strains, last, lead to the generation, at each exposure cycle, of plastic strain, localized near the exposed surface (see Fig. 6c). A plastic strain localization can be observed near the symmetry boundary condition (lower surface) corresponding to a possible overestimated value linked to the modelling assumptions. As a consequence, the trap density is modified and increases slightly at each cycle), leading to an increase of the trapped hydrogen concentration (after phase 1, $N_{T,2}$ has evolved from 8.5×10^{22} m^{-3} to 8.9×10^{22} m^{-3}, see Fig. 7b for ε_p evolution with time at point A of Fig. 3c).

During Phase 2, the heat is provided by the cooling pipes (imposed temperature of 513K). This facilitates hydrogen diffusion and detrapping. In a stress-free configuration, H transport is only driven by traps and C_L gradients, while mechanical fields (and especially compression) hardly affect the global desorption process (Fig. 7c).

6. Conclusion

It has been shown that the mechanical fields, induced by both plane strain, symmetry assumptions, and thermal expansion, have a slight effect on hydrogen fields during the different loading phases of the DFW section, and thus, on hydrogen retention. It has also been seen that boundary conditions induce plastic strain localization in their vicinity, leading to a needed interrogation on their relevance; this localization, however, has no influence on the tritium retention or the desorption flux in the DFW section.

Acknowledgements

ITER is the Nuclear Facility INB no. 174. The views and opinions expressed herein do not necessarily reflect those of the ITER Organization. This publication is provided for scientific purposes only. Its contents should not be considered as commitments from the ITER Organization as a nuclear operator in the frame of the licensing process.

This work has been performed under the auspices of the ITER Scientist Fellow Network and received funding from an ITER Organization Implementing Agreement (No. IO/IA/20/4300002270).

References

Benannoune, S., Charles, Y., Mougenot, J., Gaspérini, M., De Temmerman, G., 2020. Multidimensional finite-element simulations of the diffusion and trapping of hydrogen in plasma-facing components including thermal expansion. Phys Scr T171, 014011. doi:10.1088/1402-4896/ab4335

Bockris, J.O., Beck, W., Genshaw, M.A., Subramanyan, P.K., Williams, F.S., 1971. The effect of stress on the chemical potential of hydrogen in iron and steel 19, 1209–1218. doi:10.1016/0001-6160(71)90054-X

Chandrasekaran, H., M'Saoubi, R., Chazal, H., 2005. Modelling of material flow stress in chip formation process from orthogonal milling and split hopkinson bar tests. Mach Sci Technol 9, 131–145.

Charles, Y., Nguyen, T.H., Gaspérini, M., 2017. Comparison of hydrogen transport through pre-deformed synthetic polycrystals and homogeneous samples by finite element analysis. Int J Hydrog Energy 42, 20336–20350. doi:10.1016/j.ijhydene.2017.06.016

Giacomin, T., Delhom, D., Drevon, J.M., Guirao, J., Iglesias, S., Jourdan, T., Loesser, D., Maquet, P., Ordieres, J., Pak, S., Proust, M., Smith, M., Udintsev, V.S., Vacas, C., Walsh, M.J., Zhai, Y., 2015. Engineering requirements due to the ESP/ESPN regulation apply at the port plug for ITER diagnostic system. Fusion Eng Des 98-99, 1488–1491.

Guillermain, D., 2016. ITER Report T2YEND.

Hodille, E.A., Fernandez, N., Piazza, Z.A., Ajmalghan, M., Ferro, Y., 2018. Hydrogen supersaturated layers in H/D plasma-loaded tungsten: A global model based on thermodynamics, kinetics and density functional theory data. Phys Rev Mater 2, 093802.

Johnson, G.R., Cook, W.H., 1983. A constitutive model and data for materials subjected to large strains, high strain rates, and high temperatures, in: American Defense Preparedness Association, Koninklijk Instituut van Ingenieurs (Netherlands) (Eds.). Presented at the 7th International Symposium on Ballistics, the Hague, the Netherlands, pp. 541–547.

Khodak, A., Loesser, G., Zhai, Y., Udintsev, V., Klabacha, J., Wang, W., Johnson, D., Feder, R., 2017. Numerical Analysis of Coolant Flow and Heat Transfer in ITER Diagnostic First Wall. Fusion Sci Technol. doi:10.13182/FST14-955

Kumnick, A.J., Johnson, H.H., 1980. Deep trapping states for hydrogen in deformed iron. Acta Metall 28, 33–39. doi:10.1016/0001-6160(80)90038-3

Li, J.C.M., Oriani, R.A., Darken, L.S., 1966. The Thermodynamics of Stressed Solids. Z Phys Chem 49, 271–290. doi:10.1524/zpch.1966.49.3_5.271

Loesser, G.D., Pitcher, C.S., Feder, R., Johnson, D., Pak, S., Walsh, M., Zhai, Y., 2017. ITER Diagnostic First Wall. Fusion Sci Technol. doi:10.13182/FST12-558

McNabb, A., Foster, P.K., 1963. A new analysis of the diffusion of hydrogen in iron and ferritic steels. Trans Metall Soc AIME 227, 618–627.

Penzhorn, R.D., Torikai, Y., Watanabe, K., Matsuyama, M., Perevezentsev, A., 2012. On the fate of tritium in thermally treated stainless steel type 316L. J Nucl Mater 429, 346–352. doi:10.1016/j.jnucmat.2012.03.012

Sayman, O., Sen, F., Celik, E., Arman, Y., 2009. Thermal stress analysis of Wc–Co/Cr–Ni multilayer coatings on 316L steel substrate during cooling process. Mater Des 30, 770–774. doi:10.1016/j.matdes.2008.06.004

Simulia, 2011. Abaqus Analysis User's Manual. Dassault System.

Smith, M., Zhai, Y., Loesser, G., Wang, W., Udintsev, V., Giacomin, T., Khodak, A., Johnson, D., Feder, R., Klabacha, J., 2017. Analysis of ITER Upper Port Diagnostic First Walls. Fusion Sci Technol. doi:10.13182/FST14-990

Sofronis, P., McMeeking, R.M., 1989. Numerical analysis of hydrogen transport near a blunting crack tip. J Mech Phys Solids 37, 317–350. doi:10.1016/0022-5096(89)90002-1

Umbrello, D., M'Saoubi, R., Outeiro, J.C., 2007. The influence of Johnson–Cook material constants on finite element simulation of machining of AISI 316L steel. Int J Mach Tool Manu 47, 462–470. doi:10.1016/j.ijmachtools.2006.06.006

Vasikaran, E., Charles, Y., Gilormini, P., 2020. Implementation of a reaction-diffusion process in the Abaqus finite element software. Mech Indus 21, 508. doi:10.1051/meca/2020010